RESEARCH ARTICLE

National Science Review
13: nwaf472, 2026
https://doi.org/10.1093/nsr/nwaf472
Advance access publication 31 October 2025

[1]Interdisciplinary Materials Research Center, School of Materials Science and Engineering, Tongji University, Shanghai 201804, China; [2]Laboratory of Organic Electronics, Department of Science and Technology, Linköping University, Norrköping 60174, Sweden; [3]Wallenberg Initiative Materials Science for Sustainability, Department of Science and Technology, Linköping University, Norrköping 60174, Sweden; [4]Department of Chemistry, University of Helsinki, Helsinki FI-00014, Finland; [5]Department of Physics and Astronomy, Uppsala University, Uppsala SE-75120, Sweden and [6]Faculty of Chemistry, Wroclaw University of Science and Technology, Wroclaw PL-50370, Poland

***Corresponding authors**. E-mails: glib.baryshnikov@liu.se; xuwei@tongji.edu.cn

[†]Equally contributed to this work.

Received 12 October 2025; **Accepted** 30 October 2025

CHEMISTRY

Special Topic: Molecular Quantum Materials

Tuning aromaticity of cyclocarbons by heteroatom doping: $C_{12}S$ and $C_{12}N$

Luye Sun[1,†], Yuan Guo[1,†], Ihor Sahalianov[2,3,†], Zheng Zhou[1,†], Wei Zheng[1,†], Wenzhi Xiang[1], Yumeng Guo[1], Yuanhao Feng[1], Rashid Valiev[4], Artem Kuklin[5], Hans Ågren[5,6], Glib V. Baryshnikov[2,3,*] and Wei Xu[1,*]

ABSTRACT

Cyclo[*n*]carbons (C_n) have sparked substantial interest among experimentalists and theoreticians owing to their elusive geometric structures and unique aromaticity. Composed of two-coordinated sp-hybridized carbon atoms, C_n thus forms two perpendicular conjugated π-electron systems, i.e. out-of-plane and in-plane. Till now, on-surface generated cyclocarbons are either doubly aromatic or doubly anti-aromatic, as the number of electrons within out-of-plane and in-plane π systems was equal. Doping with heteroatoms allows one to create two π systems with different numbers of electrons, and to tune the aromaticity. Herein, we successfully generated two heteroatom-doped cyclocarbons, $C_{12}S$ and $C_{12}N$, and characterized their chemical and electronic structures. Calculations show that $C_{12}S$ exhibits an out-of-plane (14 *e*) aromatic and in-plane (12 *e*) anti-aromatic character, resulting in a total non-aromaticity. For $C_{12}N$, the out-of-plane (14 *e*) aromatic and in-plane (13 *e*) non-aromatic characters lead to total aromaticity. Doping with heteroatoms may open up the field of aromaticity engineering within cyclocarbons.

Keywords: molecular carbon allotrope, cyclocarbon, doubly aromatic, heteroatom doping, on-surface synthesis, atom manipulation

INTRODUCTION

Cyclo[*n*]carbons (C_n), a family of molecular carbon allotropes, have attracted significant attention owing to their elusive geometric structures and unique aromaticity [1–17]. C_n possesses two perpendicular conjugated π-electron systems that are formed by the alternating triple and single bonds (or consecutive double bonds): one is in-plane and the other perpendicular to the molecular plane (i.e. out-of-plane) (Fig. 1a and b). As a natural consequence of their origin from sp-hybridized carbons, all such compounds made to date have had the same number of electrons in the two π systems. Thus, they were either doubly aromatic or doubly anti-aromatic. For example, C_6 [18], C_{10} [19], C_{14} [19], C_{18} [20,21], and C_{26} [22] are all doubly aromatic (Fig. 1c and d); C_{12} [23], C_{13} [22], C_{16} [24], and C_{20} [23] are all doubly anti-aromatic (Fig. 1e and f).

Doping with heteroatoms opens the possibility of breaking this parity, because heteroatoms (i.e. S, N) have a lone pair in either the in-plane or out-of-plane system, but not both. Thus, exchanging a carbon atom or adding a heteroatom allows one to create two π systems with different numbers of electrons. Furthermore, it allows one to create systems with even numbers of electrons but odd numbers of atoms, or vice versa. Our calculations predict that S or N heteroatom doping into cyclocarbons (e.g. doubly anti-aromatic C_{12}) could significantly influence its geometric and electronic structures, and tune its aromaticity. Herein it is shown that $C_{12}S$ exhibits out-of-plane aromatic and in-plane anti-aromatic characters, resulting

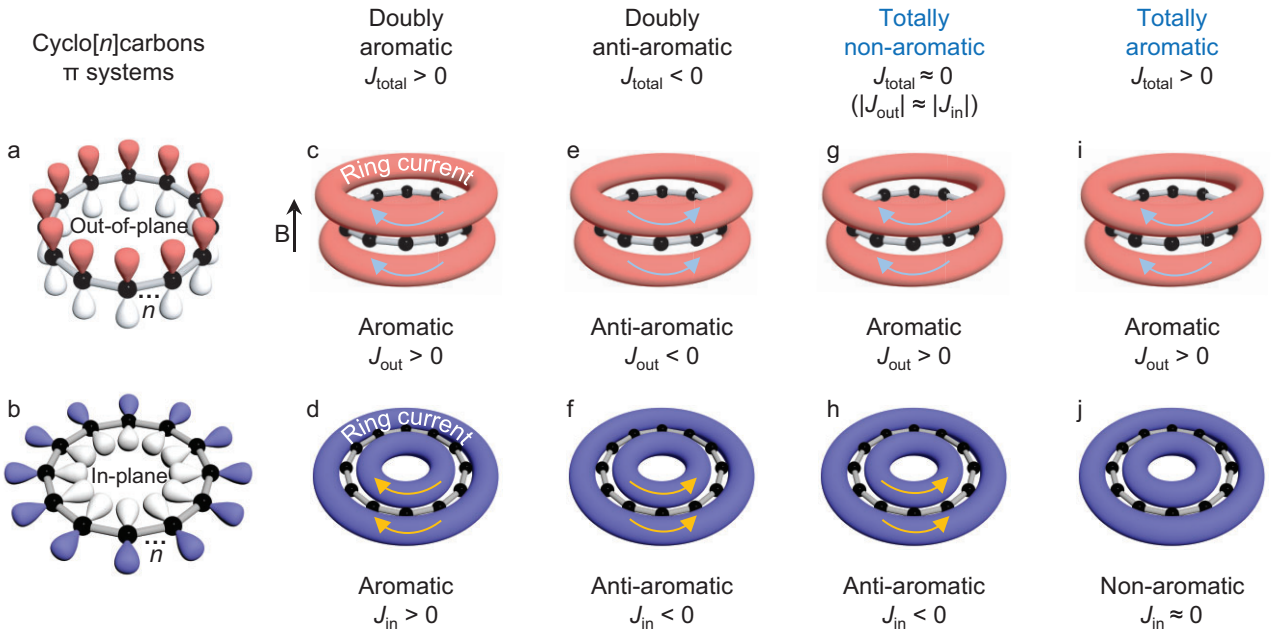

Figure 1. Two perpendicular π systems of cyclocarbons and their aromaticity. (a and b) Out-of-plane and in-plane π systems of cyclocarbons. (c and d) Doubly aromatic cyclocarbons with magnetically induced current $J_{total} > 0$ ($J_{out} > 0$, $J_{in} > 0$). (e and f) Doubly anti-aromatic cyclocarbons with $J_{total} < 0$ ($J_{out} < 0$, $J_{in} < 0$). (g and h) Totally non-aromatic cyclocarbons with $J_{total} \approx 0$ (e.g. $J_{out} > 0$, $J_{in} < 0$, and $|J_{out}| \approx |J_{in}|$). (i and j) Totally aromatic cyclocarbons with $J_{total} > 0$ (e.g. $J_{out} > 0$, $J_{in} \approx 0$). The external magnetic field B is perpendicular to the ring plane and points upward.

in a total non-aromaticity (Fig. 1g and h), which has not been reported for any cyclocarbons so far. For $C_{12}N$, the out-of-plane aromatic and in-plane non-aromatic characters lead to a total aromaticity (Fig. 1i and j), thus achieving a reversed aromaticity compared to C_{12}. It is therefore of utmost interest to experimentally generate such heteroatom-doped cyclocarbons.

The concept of aromaticity was introduced by Kekulé in 1865 [25], and nowadays, magnetic criteria of aromaticity are most widely used for molecular systems [16,22,26]. For the magnetically induced ring current J, diatropic current ($J > 0$) corresponds to aromatic character, while paratropic current ($J < 0$) corresponds to anti-aromatic one. Mathematically, we can represent the total magnetically induced current (J_{total}) of the system as a sum of the out-of-plane and in-plane currents (i.e. $J_{out} + J_{in}$) (cf. Fig. 1). As for even-numbered cyclocarbons shown in Fig. 2a to c (i.e. C_{10}, C_{12}, C_{14}), the out-of-plane and in-plane π systems both contain 10 e (14 e) for aromatic C_{10} (C_{14}) (Fig. 2a and c), with $J_{total} = 27$ nA/T ($J_{total} = 42$ nA/T) [11]. For anti-aromatic C_{12} (Fig. 2b), both out-of-plane and in-plane π systems contain 12 e, with $J_{total} = -38$ nA/T. As odd-numbered cyclocarbons, e.g. C_{13} (Fig. 2d), the out-of-plane and in-plane π systems both contain 13 e, with $J_{total} = -18$ nA/T, thus, C_{13} can be assigned as a doubly anti-aromatic cyclocarbon [22].

Herein, we focus on two heteroatom-doped cyclocarbons, i.e. S- and N-doped cyclocarbons. For $C_{12}S$ (Fig. 2e), calculations indicate out-of-plane (12 e (C) + 2 e (S), $J_{out} = 8$ nA/T) aromatic and in-plane (12 e (C), $J_{in} = -7$ nA/T) anti-aromatic character, resulting in a total non-aromaticity ($J_{total} = 1$ nA/T). For $C_{12}N$ (Fig. 2f), the out-of-plane (12 e (C) + 2 e (N), $J_{out} = 18$ nA/T) aromatic and in-plane (12 e (C) + 1 e (N), $J_{in} = 3$ nA/T) non-aromatic characters lead to a total aromaticity ($J_{total} = 21$ nA/T).

RESULTS AND DISCUSSION

Experimentally, we designed and synthesized two fully halogenated molecules (perchlorodibenzo[*b*, *d*]thiophene, $C_{12}SCl_8$, and perchloro-1H-cyclopenta[*b*]quinoline, $C_{12}NCl_9$) as the precursors for generating heteroatom-doped cyclocarbons, $C_{12}S$ and $C_{12}N$, respectively. Through scanning tunneling microscopy (STM) tip-induced dehalogenation [27,28] and accompanied ring-opening reactions, $C_{12}S$ (cf. Fig. 3a) and $C_{12}N$ (cf. Fig. 4a) were successfully generated on the surface.

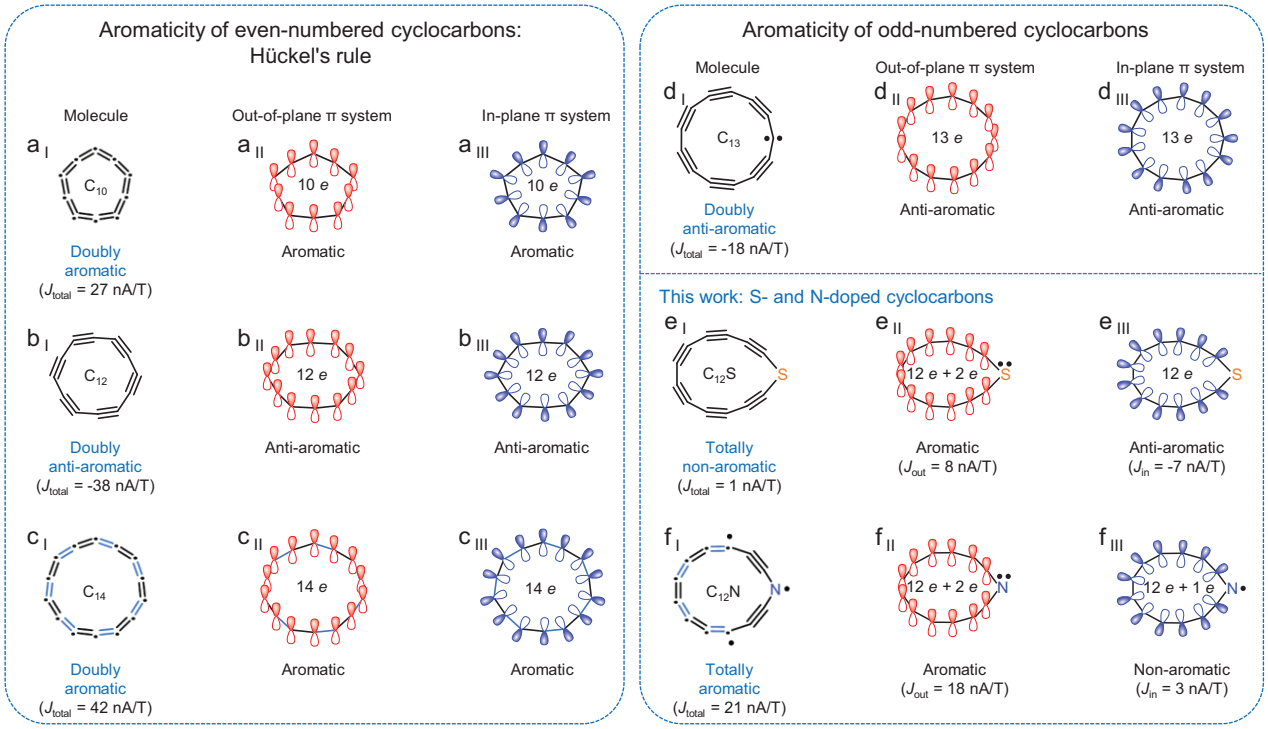

Figure 2. Aromaticity calculations of even- and odd-numbered cyclocarbons. (a_{I} to a_{III}, b_{I} to b_{III}, c_{I} to c_{III}) Aromaticity calculations of C_{10}, C_{12}, C_{14}. (d_{I} to d_{III}) Aromaticity calculations of C_{13}. (e_{I} to e_{III}, f_{I} to f_{III}) Aromaticity calculations of $C_{12}S$ and $C_{12}N$.

To generate $C_{12}S$, $C_{12}SCl_8$ molecules were introduced on the cold sample held at ~6 K. All molecules were studied on the 1 monolayer (ML) NaCl/Au(111) surface at 4.7 K. Atomic force microscopy (AFM) images (Fig. 3b $_{II}$, b $_{III}$) acquired with a CO-terminated tip revealed the skeleton of the precursor (Fig. 3b $_{I}$). To trigger dehalogenation reactions, the tip was initially positioned on a single $C_{12}SCl_8$ molecule, and retracted by 4–6 Å from a set point (typically $I = 5$ pA, $V = 0.3$ V), after that, ~4–4.5 V pulses were applied on the molecule with currents on the order of a few pA. Normally, several Cl atoms were removed, leading to the formation of typical intermediates shown in Fig. 3c and d and Fig. S2. In some intermediates the first-step retro-Bergman ring-opening reaction [19,23,29–31] has occurred, leading to the formation of a 9-membered ring containing a S atom (Fig. 3d and Fig. S2b). Subsequent voltage pulses can induce further dehalogenation and accompanied second-step retro-Bergman ring-opening reaction, leading to the formation of intermediates, e.g. $C_{12}SCl$ (Fig. 3e). AFM imaging shows a 13-membered ring with five carbon-carbon triple bonds and one Cl atom attached. Further voltage pulses could induce complete dehalogenation of intermediates (e.g. Fig. 3e), resulting in the formation of the final product $C_{12}S$ (cf. the optimized structure shown in Fig. 3f $_{I}$, Figs S3 and S4a). AFM images (Fig. 3f $_{II}$, f $_{IV}$) reveal six characteristic bright features corresponding to carbon-carbon triple bonds and a pronounced contrast at the S atom site, in consistence with AFM simulation (Fig. 3f $_{III}$). In the close tip-sample distance (Fig. S5), bright thin lines appear between triple bonds (obviously different from the cumulenic line features) [18,19], which should originate from the tip-tilting effect [32].

Moreover, we have successfully measured the differential conductance as a function of voltage, dI/dV, of a $C_{12}S$ (Fig. 3f $_{V}$). The dI/dV spectrum acquired over the $C_{12}S$ ring shows a prominent peak at ~−0.75 V. STM images (Fig. 3f $_{VI}$, f $_{VII}$) obtained at this bias voltage correspond to the PIR state, showing characteristic lobes similar to the ones of C_{20} [23]. This state could result from the superposition of the densities of the nearly energy degenerated highest occupied molecular orbitals (HOMOs) (Fig. 3f $_{VIII}$ and Fig. S6). It is considered that the peak at the PIR dominantly relates to the out-of-plane orbitals [22]. In addition, due to the energy broadening of the ionic resonances on NaCl (~0.3 V) [33], nearly degenerated orbitals could not be resolved as separate peaks in the dI/dV spectrum.

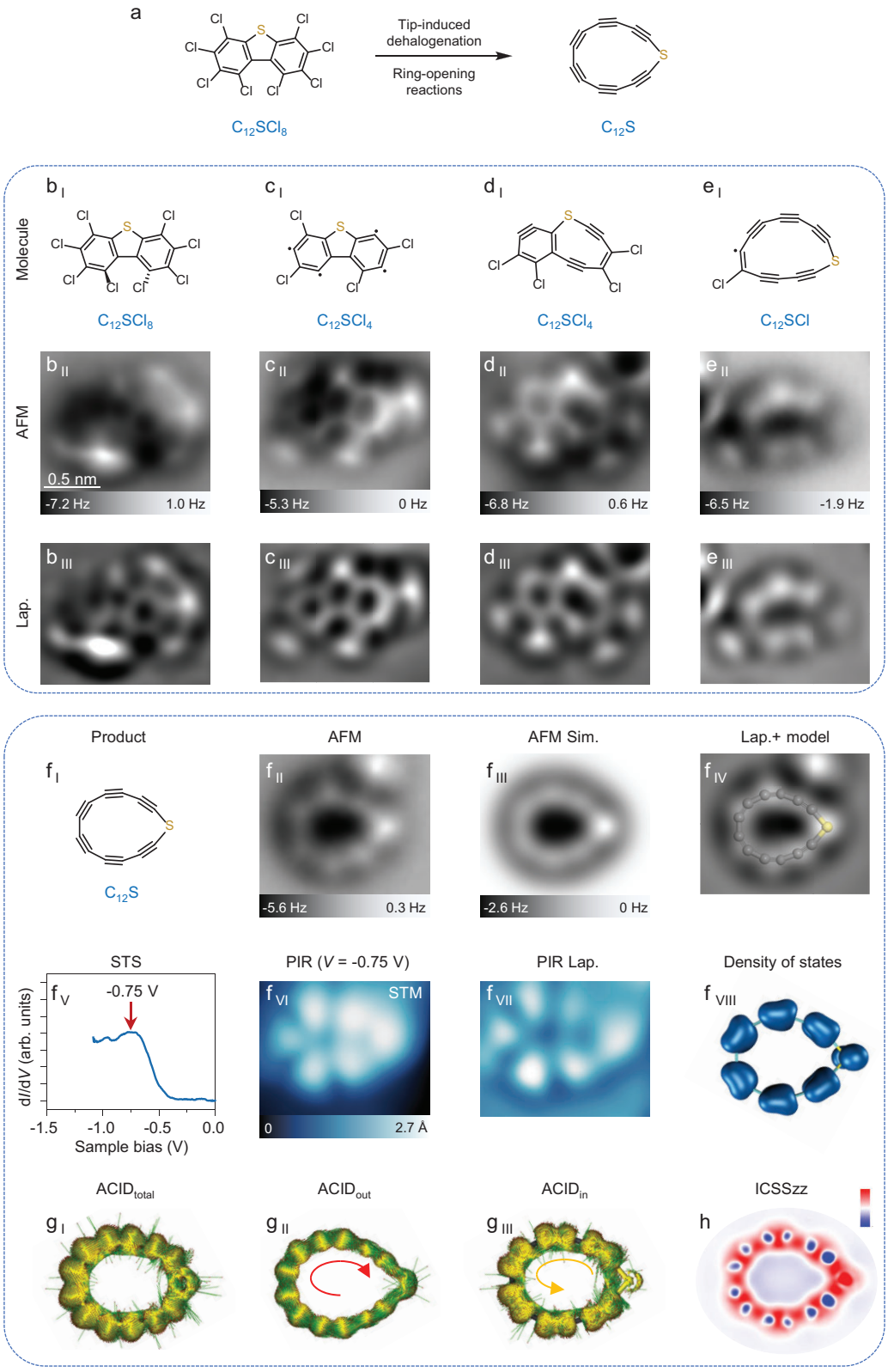

Figure 3. On-surface synthesis of $C_{12}S$ and its aromaticity calculations. (a) Reaction scheme for the formation of $C_{12}S$ by dehalogenation and ring-opening reactions. (b $_{I}$ to b $_{III}$, c $_{I}$ to c $_{III}$, d $_{I}$ to d $_{III}$, e $_{I}$ to e $_{III}$) Molecular structures, atomic force microscopy (AFM) images, and Laplace-filtered AFM images of precursor and typical

Figure 3. (*Continued*) intermediates. (f_I to f_{IV}) Molecular structure, AFM image, AFM simulation, Laplace-filtered AFM image with a superimposed model of product ($C_{12}S$). (f_V) Scanning tunneling spectroscopy (STS) of $C_{12}S$ acquired with a CO-terminated tip. The differential conductance (d*I*/d*V*) signal acquired on the $C_{12}S$ shows a peak that can be attributed to the positive ion resonance (PIR) state. (f_{VI}) STM image at PIR ($V = -0.75$ V, $I = 2$ pA). (f_{VII}) Laplace-filtered STM image. (f_{VIII}) Superposition of the densities of the nearly energy degenerated highest occupied molecular orbitals (HOMOs). (g_I to g_{III}) Total, out-of-plane and in-plane ACID plots for $C_{12}S$. (h) ICSSzz plot for $C_{12}S$. Color bar: from −60 to 60. AFM tip offsets Δz: +0.3 Å, +0.2 Å, 0 Å, −0.4 Å, −1.0 Å for b_{II} to f_{II}. Reference set points of Δz: $I = 5$ pA, $V = 0.3$ V for b_{II}, $I = 4$ pA, $V = 0.3$ V for c_{II} to e_{II}, $I = 0.5$ pA, $V = 0.3$ V for f_{II}. The scale bar in (b_{II}) applies to all experimental images. The external magnetic field is perpendicular to the ring plane and points upward.

$C_{12}NCl_9$ molecules [34] (Fig. 4b$_I$ to b$_{III}$) were introduced onto the surface to generate $C_{12}N$. Similarly, applied voltage pulses (∼4–4.5 V) can remove one or more Cl atoms, leading to the formation of typical intermediates (e.g. Fig. 4c–e). Not only the 6–6–5 skeleton, but more importantly the larger 10- and 13-membered rings of intermediates were revealed by AFM images, indicating the occurrence of first-step and second-step ring-opening reactions. Subsequent voltage pulses could induce complete dehalogenation of intermediates (e.g. Fig. 4e), resulting in the formation of the final product $C_{12}N$ (cf. the optimized structure shown in Fig. 4f$_I$, Figs S4b and S7). For $C_{12}N$, the N atom site in AFM images (Fig. 4f$_{II}$, f$_{IV}$) has a weaker contrast compared to carbon-carbon bonds [35]. AFM images at different tip heights (Fig. 4f$_{II}$ and Fig. S8) show two characteristic bright features (assigned to triple bonds) near to the N site and uniform line features (assigned to the cumulenic moiety) within $C_{12}N$, in accordance with the AFM simulation (Fig. 4f$_{III}$).

Moreover, the d*I*/d*V* spectrum (Fig. 4f$_V$) acquired over the $C_{12}N$ ring shows a prominent peak at ∼−2.25 V. STM images (Fig. 4f$_{VI}$, f$_{VII}$) obtained at this bias voltage correspond to the PIR state, showing a nearly delocalized state (i.e. no obvious lobes in comparison with $C_{12}S$) (Fig. 4f$_{VIII}$ and Fig. S9). It is still challenging to measure the negative ion resonance (NIR) of $C_{12}S$ and $C_{12}N$ due to the high mobility of the ring.

Calculations for anisotropy of the induced current density (ACID) [36] were conducted to visualize the magnetically induced current of $C_{12}S$ (Fig. 3g and Fig. S10). $ACID_{out}$ (Fig. 3g$_{II}$) and $ACID_{in}$ (Fig. 3g$_{III}$) plots indicate the presence of a diatropic current (indicated by red clockwise arrow) within the out-of-plane π system and paratropic current (indicated by yellow anti-clockwise arrow) within the in-plane π system, leading to a very small diatropic current in $ACID_{total}$ (Fig. 3g$_I$). It is found that an in-plane paratropic current is formed by avoiding the kink at the S atom, because the S atom could not provide the lone electron pair into the conjugation circuit inside the $C_{12}S$ ring, thus only in-plane 12 electrons by 12 carbon atoms are involved in the paratropic current. Iso-chemical shielding surface (ICSSzz) [37] plots (Fig. 3h and Fig. S11) further confirm the presence of diatropic out-of-plane and paratropic in-plane currents.

For $C_{12}N$, $ACID_{out}$ (Fig. 4g$_{II}$) and $ACID_{in}$ (Fig. 4g$_{III}$) plots indicate the presence of a large diatropic current (indicated by red clockwise arrow) within the out-of-plane π system and very small diatropic current within the in-plane π system, leading to a diatropic current (indicated by red clockwise arrow) in $ACID_{total}$ (Fig. 4g$_I$ and Fig. S12). Compared with $C_{12}S$, the N atom provides only one electron into the in-plane conjugation circuit of the $C_{12}N$ ring, resulting in a 13π-electron very weak aromatic system, while the out-of-plane 14π-electron aromatic system provides the dominant diatropic contribution to the total current. Moreover, the $ICSS_{zz}$ plots only show a diatropic contribution (Fig. 4h and Fig. S13). The results of the aromaticity calculations of $C_{12}S$ and $C_{12}N$ are in consistence with the geometries and electronic state revealed by AFM and STM imaging (Figs 3f and 4f). Specifically, compared with the non-aromatic $C_{12}S$, aromatic $C_{12}N$ exhibits reduced bond-length alternations and more delocalized PIR states.

CONCLUSION

In conclusion, we have successfully generated two heteroatom S- and N-doped cyclocarbons, i.e. $C_{12}S$ and $C_{12}N$, via the on-surface synthesis method. The doped heteroatoms result in different numbers of electrons within the out-of-plane and in-plane conjugated π systems, and tune the aromaticity. Such a strategy of introducing heteroatoms may open up the field of aromaticity engineering within cyclocarbons.

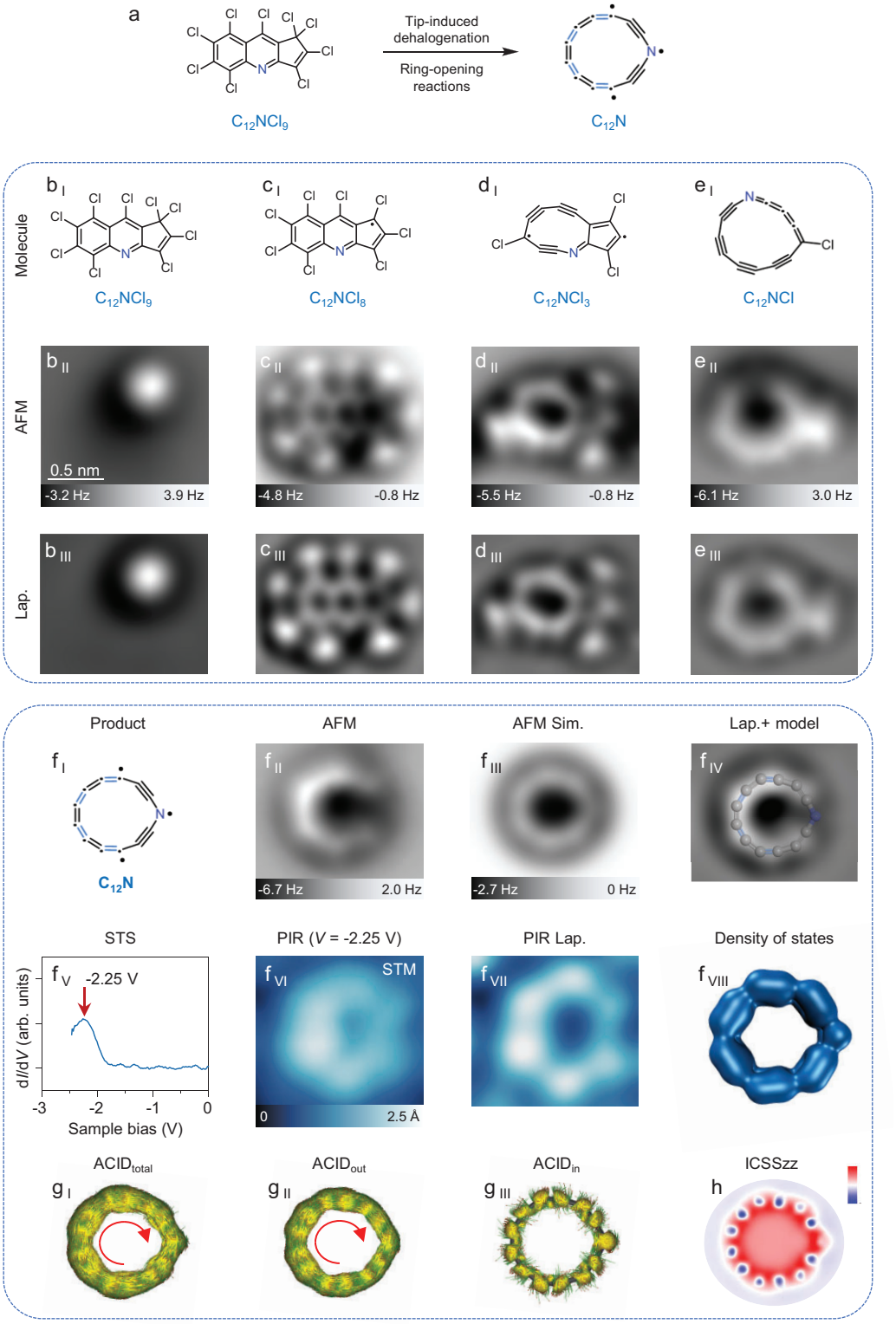

Figure 4. On-surface synthesis of $C_{12}N$ and its aromaticity calculations. (a) Reaction scheme for the formation of $C_{12}N$ by dehalogenation and ring-opening reactions. (b_{I} to b_{III}, c_{I} to c_{III}, d_{I} to d_{III}, e_{I} to e_{III}) Molecular structures, atomic force microscopy (AFM) images, and Laplace-filtered AFM images of precursor and typical intermediates. (f_{I} to f_{IV}) Molecular structure, AFM image, AFM simulation, Laplace-filtered AFM image with a superimposed model of product ($C_{12}N$). (f_{V}) Scanning tunneling spectroscopy (STS) of $C_{12}N$ acquired with a CO-terminated tip. The d*I*/d*V* signal acquired on the $C_{12}N$ shows a peak that can be attributed to the PIR state. (f_{VI}) STM image at PIR ($V = -2.25$ V, $I = 2$ pA). (f_{VII}) Laplace-filtered STM image. (f_{VIII}) Superposition of the densities of the nearly energy degenerated highest

Figure 4. (*Continued*) occupied molecular orbitals (HOMOs). ($g_{\ I}$ to $g_{\ III}$) Total, out-of-plane and in-plane ACID plots for $C_{12}N$. (h) ICSSzz plot for $C_{12}N$. Color bar: from −100 to 100. AFM tip offsets Δz: 0 Å, −1.4 Å, −1.4 Å, −1.3 Å, −1.5 Å for $b_{\ II}$ to $f_{\ II}$. Reference set points of Δz: $I = 0.5$ pA, $V = 0.3$ V for $b_{\ II}$ to $f_{\ II}$. The scale bar in ($b_{\ II}$) applies to all experimental images. The external magnetic field is perpendicular to the ring plane and points upward.

SUPPLEMENTARY DATA

Supplementary data are available at *NSR* online.

FUNDING

This work was supported by the National Natural Science Foundation of China (22125203 and 22402149), the National Key R&D Program of China (2023YFE0101900), the Ministry of Science and Technology of the People's Republic of China, and the Shanghai Science and Technology Program (24ZR1470000). This work was also partially supported by the National Academic Infrastructure for Supercomputing in Sweden (NAISS 2025/5-140, 2024/5-552) at the National Supercomputer Centre of Linköping University (Sweden) and PDC Dardel partially funded by the Swedish Research Council (2022-06 725), the Wallenberg Initiative Materials Science for Sustainability (WISE) funded by the Knut and Alice Wallenberg Foundation, the Swedish Research Council (2024-05 286), Swedish Government Strategic Research Area in Materials Science on Advanced Functional Materials at Linköping University (Faculty grant SFO-Mat-LiU no. 2009-00 971) funded by the European Union (ERC, LUMOR, 101077 649). Views and opinions expressed are however those of the authors only and do not necessarily reflect those of the European Union or the European Research Council Executive Agency. Neither the European Union nor the granting authority can be held responsible for them. R.V. thanks the Academy of Finland through Projects 346369.

AUTHOR CONTRIBUTIONS

W.X. conceived the research. L.S., Y.G. and W.X. performed the STM/AFM experiments. Z.Z., W.Z., Y.G. and Y.F. synthesized the $C_{12}SCl_8$ and $C_{12}NCl_9$ molecules. I.S., R.V., A.K., H.Å. and G.B. carried out the calculations. All authors contributed to writing and discussing the manuscript.

***Conflict of interest statement*.** None declared.

REFERENCES

1. Parent DC and McElvany SW. Investigations of small carbon cluster-ion structures by reactions with hydrogen cyanide. *J Am Chem Soc* 1989; **111**: 2393–401.
2. Van Orden A and Saykally RJ. Small carbon clusters: spectroscopy, structure, and energetics. *Chem Rev* 1998; **98**: 2313–57.
3. Grutter M, Wyss M, Riaplov E *et al.* Electronic absorption spectra of linear C_6, C_8 and cyclic C_{10}, C_{12} in neon matrices. *J Chem Phys* 1999; **111**: 7397–401.
4. Diederich F. Carbon scaffolding: building acetylenic all-carbon and carbon-rich compounds. *Nature* 1994; **369**: 199–207.
5. Pitzer KS and Clementi E. Large molecules in carbon vapor. *J Am Chem Soc* 1959; **81**: 4477–85.
6. Parasuk V, Almlof J, Feyereisen MW. The [18] all-carbon molecule: cumulene or polyacetylene? *J Am Chem Soc* 1991; **113**: 1049–50.
7. Torelli T and Mitas L. Electron correlation in C_{4N+2} carbon rings: aromatic versus dimerized structures. *Phys Rev Lett* 2000; **85**: 1702–5.
8. Arulmozhiraja S and Ohno T. CCSD calculations on C_{14}, C_{18}, and C_{22} carbon clusters. *J Chem Phys* 2008; **128**: 114301.
9. Remya K and Suresh CH. Carbon rings: a DFT study on geometry, aromaticity, intermolecular carbon-carbon interactions and stability. *RSC Adv* 2016; **6**: 44261–71.
10. Baryshnikov GV, Valiev RR, Kuklin AV *et al.* Cyclo[18]carbon: insight into electronic structure, aromaticity, and surface coupling. *J Phys Chem Lett* 2019; **10**: 6701–5.
11. Baryshnikov GV, Valiev RR, Nasibullin RT *et al.* Aromaticity of even-number cyclo[*n*]carbons ($n = 6$–100). *J Phys Chem A* 2020; **124**: 10849–55.
12. Charistos ND and Muñoz-Castro A. Induced magnetic field in sp-hybridized carbon rings: analysis of double aromaticity and antiaromaticity in cyclo[2*N*]carbon allotropes. *Phys Chem Chem Phys* 2020; **22**: 9240–9.
13. Brémond E, Pérez-Jiménez AJ, Adamo C *et al.* Stability of the polyynic form of C_{18}, C_{22}, C_{26}, and C_{30} nanorings: a challenge tackled by range-separated double-hybrid density functionals. *Phys Chem Chem Phys* 2022; **24**: 4515–25.
14. Li M, Gao Z, Han Y *et al.* Potential molecular semiconductor devices: cyclo-C_n ($n = 10$ and 14) with higher stabilities and aromaticities than acknowledged cyclo-C_{18}. *Phys Chem Chem Phys* 2020; **22**: 4823–31.
15. Liu Z, Lu T, Chen Q. An sp-hybridized all-carboatomic ring, cyclo[18]carbon: bonding character, electron delocalization, and aromaticity. *Carbon* 2020; **165**: 468–75.
16. Baryshnikov GV, Valiev RR, Valiulina LI *et al.* Odd-number cyclo[*n*]carbons sustaining alternating aromaticity. *J Phys Chem A* 2022; **126**: 2445–52.
17. Fowler PW, Mizoguchi N, Bean DE *et al.* Double aromaticity and ring currents in all-carbon rings. *Chem Eur J* 2009; **15**: 6964–72.
18. Sun L, Guo Y, Xiang W *et al.* On-surface synthesis and characterization of linear and cyclic C_6. *Nat Synth* 2025; **4**: 940–6.
19. Sun L, Zheng W, Gao W *et al.* On-surface synthesis of aromatic cyclo[10]carbon and cyclo[14]carbon. *Nature* 2023; **623**: 972–6.
20. Kaiser K, Scriven LM, Schulz F *et al.* An sp-hybridized molecular carbon allotrope, cyclo[18]carbon. *Science* 2019; **365**: 1299–301.

21. Scriven LM, Kaiser K, Schulz F *et al.* Synthesis of cyclo[18]carbon via debromination of $C_{18}Br_6$. *J Am Chem Soc* 2020; **142**: 12921–4.
22. Albrecht F, Rončević I, Gao Y *et al.* The odd-number cyclo[13]carbon and its dimer, cyclo[26]carbon. *Science* 2024; **384**: 677–82.
23. Sun L, Zheng W, Kang F *et al.* On-surface synthesis and characterization of anti-aromatic cyclo[12]carbon and cyclo[20]carbon. *Nat Commun* 2024; **15**: 7649.
24. Gao Y, Albrecht F, Rončević I *et al.* On-surface synthesis of a doubly anti-aromatic carbon allotrope. *Nature* 2023; **623**: 977–81.
25. Kekulé A. Sur la constitution des substances aromatiques. *Bull Soc Chim Paris* 1865; **3**: 98–110.
26. Merino G, Solà M, Fernández I *et al.* Aromaticity: quo Vadis. *Chem Sci* 2023; **14**: 5569–76.
27. Pavliček N, Schuler B, Collazos S *et al.* On-surface generation and imaging of arynes by atomic force microscopy. *Nat Chem* 2015; **7**: 623–8.
28. Pavliček N, Gawel P, Kohn DR *et al.* Polyyne formation via skeletal rearrangement induced by atomic manipulation. *Nat Chem* 2018; **10**: 853–8.
29. Jones RR and Bergman RG. *p*-benzyne. Generation as an intermediate in a thermal isomerization reaction and trapping evidence for the 1,4-benzenediyl structure. *J Am Chem Soc* 1972; **94**: 660–1.
30. Schuler B, Fatayer S, Mohn F *et al.* Reversible Bergman cyclization by atomic manipulation. *Nat Chem* 2016; **8**: 220–4.
31. Albrecht F, Fatayer S, Pozo I *et al.* Selectivity in single-molecule reactions by tip-induced redox chemistry. *Science* 2022; **377**: 298–301.
32. Hapala P, Kichin G, Wagner C *et al.* Mechanism of high-resolution STM/AFM imaging with functionalized tips. *Phys Rev B* 2014; **90**: 085421.
33. Repp J, Meyer G, Stojković SM *et al.* Molecules on insulating films: scanning-tunneling microscopy imaging of individual molecular orbitals. *Phys Rev Lett* 2005; **94**: 026803.
34. Dobrowolski MA, Cyranski MK, Wrobel Z. Cyclic π-electron delocalization in non-planar linear acenes. *Phys Chem Chem Phys* 2016; **18**: 11813–20.
35. Kawai S, Nakatsuka S, Hatakeyama T *et al.* Multiple heteroatom substitution to graphene nanoribbon. *Sci Adv* 2018; **4**: eaar7181.
36. Geuenich D, Hess K, Köhler F *et al.* Anisotropy of the induced current density (ACID), a general method to quantify and visualize electronic delocalization. *Chem Rev* 2005; **105**: 3758–72.
37. Klod S and Kleinpeter E. *Ab initio* calculation of the anisotropy effect of multiple bonds and the ring current effect of arenes—Application in conformational and configurational analysis. *J Chem Soc, Perkin Trans 2* 2001; 1893–8.